Research on Chemical Intermediates (2023) 49:3627–3643
https://doi.org/10.1007/s11164-023-05048-w

Adsorptive and oxidative removal of naproxen and diclofenac using Ag NPs, Cu NPs and Ag/Cu NPs

Muradiye Şahin[1] Yasin Arslan[2]

Received: 27 March 2023 / Accepted: 5 June 2023 / Published online: 19 June 2023

Abstract

Considering the removal potential of anti-inflammatory drugs, it was observed that diclofenac and naproxen were more difficult to separate from sample matrix with respect to other anti-inflammatory drugs. As a result of the measurements of these drugs in the river, groundwater and treatment plant effluent streams, it was determined that 37% of the total chemical was retained on colloidal non-precipitating particles, and the remaining part was in dissolved form. In this study, the catalytic activity and adsorption performance of inexpensive, simple, environmentally friendly and innovative adsorbents such as Ag NPs, Cu NPs and Ag/Cu NPs synthesized at the first time by a green synthesis method using weed plant Helichrysum arenarium extract were investigated in the removal of naproxen and diclofenac drugs from aqueous solution. The structure of the obtained nanoparticles was characterized by UV–Vis, FT-IR, XRD, SEM–EDX, TEM and BET analyzes. It was determined that Cu NPs showed both the highest catalytic activity and the highest adsorption property among the synthesized other nanoparticles. The synergistic effect was investigated in detail by combining adsorption and catalytic wet peroxidation processes to perform with faster and higher efficiency of drug removal. Based on experimental results, Cu NPs degraded 84%, 91% and 75% of naproxen, diclofenac and naproxen+diclofenac drugs, respectively, and showed strong selectivity against diclofenac after 50 min.

Extended author information available on the last page of the article

Graphical abstract

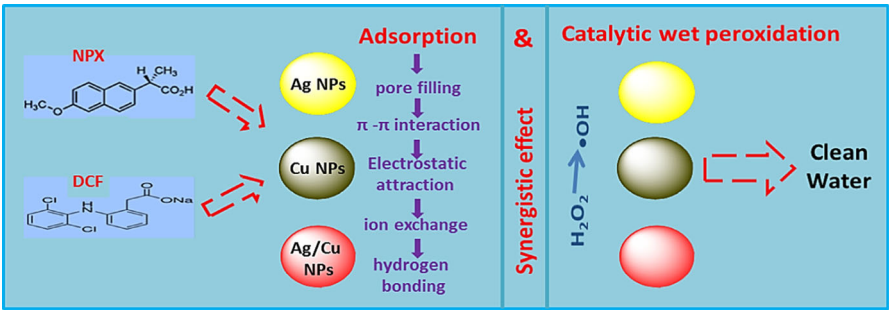

Keywords Nanocatalyst · Synergistic effect · Adsorption · Drug removal · Catalytic wet peroxidation

Introduction

With the development of science, industry and technology, the increasing release of various organic pollutants and biological wastes into the ecosystem is an important concern. [1, 2]. In the last few years, the use of drugs in the field of medicine to protect human and animal health has led to an undesirable accumulation of pharmaceutical wastes in the environment. Most of these pharmaceuticals have a stable structure and their removal is not possible with conventional purification methods. A significant number of these compounds have been detected frequently in different aquatic environments (wastewater, surface water, drinking water and groundwater) and solids (sludge, soil and sediments) [3]. When the current studies on the subject are examined, it is understood that researchers have an intense interest in the removal of pharmaceutical residues due to their excessive formation and permanent character in the environment. Long-term and low-dose exposure to pharmaceutical products in the environment leads to adverse effects on target organisms such as endocrine disruption, chronic toxicity and antibiotic resistance [4]. Naproxen, ibuprofen and diclofenac are acidic pharmaceuticals belonging to the NSAID class [5]. Diclofenac is a resistant and bioaccumulative pharmaceutical compound widely used as an anti-inflammatory in humans and veterinary medicine [6–8]. It can be found in wastewater through the destruction of urine and animal skeletons, spread throughout the ecosystem food chain [9, 10]. Naproxen has analgesic and anti-inflammatory properties [11] so it is consumed in large quantities by humans and animals [12]. About 72% of the naproxen excreted from the body can be easily broken down and released into water resources [13]. Antibiotic residues moving from concentration ranges from ng/L to mg/L levels in aquatic environments on a global scale [14] pose a high risk for all living organisms in seas. According to the current data of the World Health Organization (WHO), it is predicted that more than 10,000,000 people may die by 2050 due to antibiotic-resistant infections [15].

However, methods are gradually being developed for the efficient removal of organic pharmaceutical from wastewater. To date, various methods such as biodegradation [16], coagulation–flocculation [17], biofiltration [18], chlorination [19], ozonation [20], photocatalysis [21–23], advanced oxidation processes (AOPs) [24] and adsorption [25] have been widely used to remove and/or decompose pharmaceutical contaminants from aqueous solutions. Although the adsorption process is used to remove many pollutants in current studies, studies in which innovative adsorbents are used to remove drugs, are very limited in the literature. Activated carbon, carbon nanotubes, bentonite and some ions are the most commonly used adsorbents in the removal of drugs in studies carried out to date. Investigation of innovative adsorbents in drug removal from aquatic environments will contribute to the literature. Therefore, Ag, Ag/Cu and Cu NPs nanoparticles were synthesized as some alternative particles to remove nonsteroidal anti-inflammatory drugs, such as naproxen and diclofenac in this study.

Catalytic wet peroxidation (CWPO) and adsorption are the most preferred methods for drug removal from aqueous solutions due to the relatively simple equipment required, their ability to operate under environmental conditions, their ability to remove most organic pollutants, their low cost and their environmentally friendly nature. In this regard, metal nanoparticles are popular as catalysts/adsorbent due to their excellent catalysis and good sensor properties, large surface area and high reactivity [26]. Bimetallic nanoparticles contain two different metal atoms in a single nanoparticle and are predicted to exhibit novel properties due to the synergistic effects of the combined metals, as well as the combination of properties of the two separate metals [27]. The distribution of metal atoms defines the final structure and performance activity of nanoparticles [28]. Various physical and chemical methods have been used in the synthesis of bimetallic nanoparticles, and the most widely used method for the preparation of bimetallic nanoparticles is chemical reduction in aqueous solutions, which allows to obtain bimetallic nanoparticles in different forms [27]. However, these methods are expensive and often require hazardous materials [29, 30]. The green method is preferred because it is a safe, inexpensive and easy process. Algae, bacteria, fungi and plants are bioreactors used for green synthesis of metal nanoparticles [22]. Among them, plants offer significant advantages over others due to their availability, cost and safety for both the environment and living organisms [30]. Plant extracts contain metabolites that can reduce metal ions and facilitate the formation of nanoparticles. In addition, large-scale synthesis can be performed by using plant extracts for nanoparticle synthesis [31].

In this study, the synthesis and characterization of silver and copper nanoparticles (Ag NPs, Cu NPs) and silver/copper bimetallic nanoparticles (Ag/Cu NPs) from weed plant Helichrysum arenarium extract with a cheap, simple and environmentally friendly by green method were reported. The aim of this study was to examine the both separate and competitive removal of nonsteroidal anti-inflammatory drugs (naproxen (NPX) and diclofenac (DCF)) from aqueous solution by green synthesized metallic/bimetallic nanoparticles. Here, we report the catalytic activity, adsorption performance, selectivity and kinetic data of metallic (Ag NPs, Cu NPs) and bimetallic (Ag/Cu NPs) nanoparticles for both NPX and DCF removal from aqueous solution. As far as we can ascertain, this is the first study in the literature in terms of

examining the synergistic effect of the hybrid adsorption/oxidation of NPX and DCF by Ag NPs, Cu NPs and Ag/Cu NPs synthesized for the first time using weed plant Helichrysum arenarium extract.

Materials and methods

Materials and reagents

Silver nitrate ($AgNO_3$) was purchased from Fluka. Diclofenac sodium ($C_{14}H_{10}Cl_2NNaO_2$) and sodium chloride (NaCl) were purchased from Sigma-Aldrich. Naproxen sodium ($C_{14}H_{13}NaO_3$) was purchased from Acros Organics. Copper (II) sulfate pentahydrate ($CuSO_4.5H_2O$) was purchased from Indosaw. Hydrogen peroxide (H_2O_2) was purchased from Merck. Double distilled water was used throughout the all experimental studies (18.2 MΩ cm). All of the materials were in analytical reagent grade and utilized as received without any purification.

Characterization techniques

The chemical and morphological characterizations of the all nanoparticles were realized by Shimadzu UV-1800 (UV–Vis), Perkin Elmer Fronter model FT-IR, Bruker D8 Advance model X-ray diffraction (XRD) with a Cu K_α radiation source in 2θ range from 10° to 90°, TEM-120 kV transmission electron microscope (TEM), Carl Zeiss EVO-LS 10 scanning electron microscope (SEM) and Quantachrome Quadrasorb SI Brunauer–Emmett–Teller (BET) specific surface area.

Synthesis of catalysts/adsorbents

To obtain extract, 1 g of weed plant Helichrysum arenarium was gauged and added to 50 mL of distilled water. The blend was stirred continuously at 25 °C for 5 h. After grinding, the mixture was separated with a Whatman No. 1 filter paper. Moreover, 0.1 M 50 mL of silver nitrate solution was prepared. Then, for the preparation of Ag NPs, the weed plant Helichrysum arenarium extract (5 mL) was added to 0.1 M 45 mL of $AgNO_3$ at pH=5 [32]. For the synthesis of Cu NPs, 100 mL solution including 0.1 M 50 mL copper (II) sulfate pentahydrate was prepared and 7 mL of the weed plant Helichrysum arenarium extract was added to the prepared solution at pH=9. For the synthesis of Ag/Cu NPs, 100 mL solution including 1.69 g $AgNO_3$ and 2.49 g $CuSO_4.5H_2O$ was prepared and 10 mL of the plant extract was added to the prepared solution. Then, they were mixed at room temperature for 30 min at 500 rpm on a magnetic stirrer and left overnight to settle. At the end of this period, the pH=9 was adjusted and left to settle again for 2 h so that no non-precipitated Cu NPs remained. The resulting Ag NPs, Cu NPs and Ag/Cu NPs were separated from the filtrate with a Whatman No. 1 filter paper (90 mm, 82 g/m^2 and pore size: 15–19 μm) and washed 3 times with distilled water and dried in an oven [33, 34].

Adsorption experiments

Adsorption of NPX, DCF and NPX+DCF on nanoadsorbents was carried out using the batch adsorption method. For this, 25 mg adsorbents were separately mixed with 50 mL of 20 mg/L drug solutions in 100 mL beakers at pH=4.5 and 298 K. Then all tubes were mixed at 250 rpm for 90 min and the drug concentrations remaining unadsorbed in the solution were determined by measuring the absorbances for NPX and DCF at 272 nm and 254 nm, respectively, with a UV–Vis spectrophotometer [33, 34].

Catalytic wet peroxidation of NPX, DCF and NPX+DCF

In CWPO experiments, 20 mg/L, 50 mL of NPX solution, 20 mg/L, 50 mL of DCF solution and 50 mL of 10 mg/L NPX+10 mg/L DCF mixed solution were separately stirred with a magnetic stirrer at 250 rpm throughout the experiment period. The effects of the amount of catalyst (10, 25, 50 and 75 mg), pH (3, 4.5, 8 and 10), temperature (25, 40, 55 and 70 °C) and H_2O_2 concentration (20, 30, 40 and 50% (v/v)) were investigated in order to determine catalytic activity on the decomposition of NPX and DCF with CWPO technique. The optimum experimental parameters were found to be 25 mg for the amount of catalyst, 4.5 for pH, 25 °C for temperature and 30% for H_2O_2 concentration, respectively. The oxidation experiments were carried out using these optimum experimental parameters in which the highest catalytic activity was obtained for the decomposition of NPX and DCF with CWPO technique. The catalytic process was started by adding 3 mL of freshly prepared 30% H_2O_2 and then 0.025 g nanocatalyst was added to the solution. 3 mL of sample was taken at regular intervals, separated from the catalyst by filtered, and 1 mL of distilled water was added and then UV–Vis. measurements were taken.

Results and discussion

Nanocatalysts/nanoadsorbents Structure

The peaks seen at 455 nm and 610 nm in UV–Vis. (Fig. 1a) are the characteristic peaks of Ag and Cu, respectively, and it was confirmed that the nanoparticle was successfully synthesized [30, 31]. Common drift method was used to determine the pH (pHpzc) of nanoparticles at the neutral charge point. For this, 50 mL of 0.01 M NaCl solution was placed in a closed erlenmeyer flask. The pH value was adjusted to a value between 2.0 and 8.0 by adding 0.1 M HCl and/or 0.1 M NaOH solutions. Then 0.025 g of each nanoparticle was added and the final pH was measured after 24 h under shaking at room temperature [33, 34]. The intersection point of initial pH and final pH values was determined to be pHpzc (Fig. 1b). The pHpzc values of Ag NPs, Ag/Cu NPs and Cu NPs were found to be 5.15; 5.19 and 5.58, respectively, and further studies were carried out at pH=4.5, which is below the pzc value for all adsorbents.

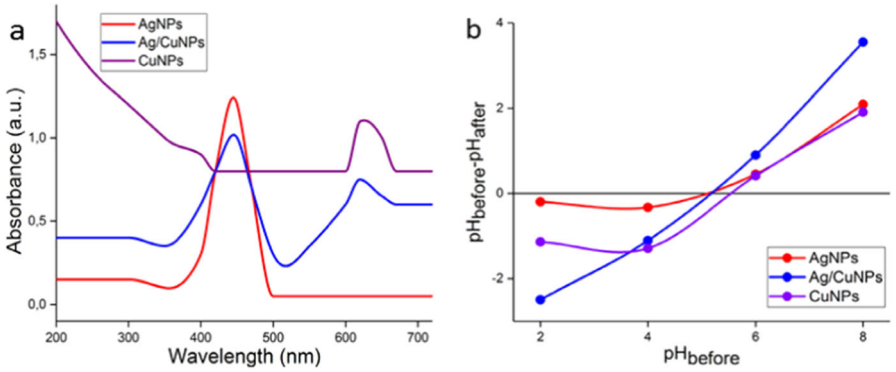

Fig. 1 **a** UV–Vis spectra of Ag NPs, Cu NPs and Ag/Cu NPs, **b** pH_{PZC} of the catalysts/adsorbents (conditions: 25 mg each nanoparticle, 50 mL 0.01 M NaCl, 25 °C and 24 h)

FT-IR analyzes of weed plant Helichrysum arenarium, Ag NPs, Ag/Cu NPs and Cu NPs are comparatively given in Fig. 2a. In the FT-IR spectra of Ag/Cu NPs and Cu NPs, the characteristic peak seen at 555 cm^{-1} is due to the stretching vibration of the Cu–O bond and the characteristic peak seen at 1010 cm^{-1} is due to the presence of Cu [35]. The peaks seen at 3447 cm^{-1} and 2859 cm^{-1} in the weed plant Helichrysum arenarium spectrum belong to –OH and –NH asymmetric vibrations, respectively; it shows that there are phenol and amine groups in the plant structure. The disappearance of these peaks in the synthesized nanoparticles shows that weed plant Helichrysum arenarium is an effective reducing agent with phenol and amine groups in the formation of nanoparticles. Apart from these, stretching vibrations of C=O bonds at 1712 cm^{-1}, C=C bonds at 1650 cm^{-1}, and characteristic peaks of CO bond at 1153 and 1021 cm^{-1} indicate that there is an ester group in the plant structure.

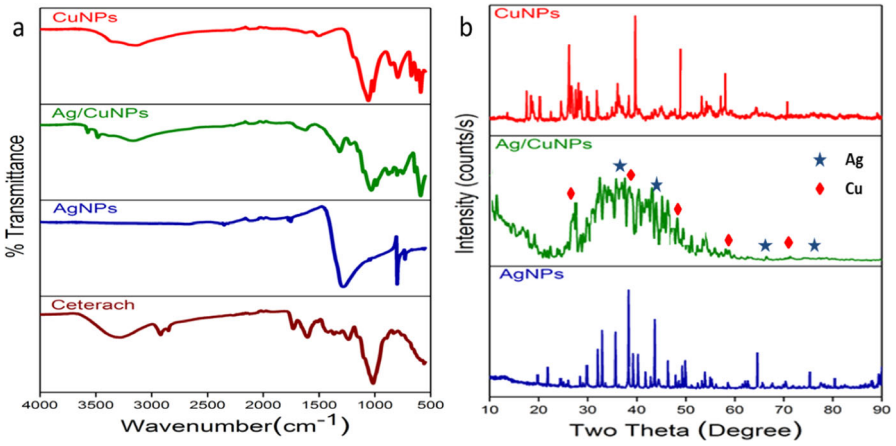

Fig. 2 **a** FT-IR and **b.** XRD spectrum of Ag NPs, Ag/Cu NPs and Cu NPs

The X-ray diffraction spectrum of Ag NPs, Ag/Cu NPs and Cu NPs is shown in Fig. 2b. As a result of the obtained diffraction spectrum, the crystal structures (111), (200), (220), (311) and (222) corresponding to 2θ=38.1°, 44.3°, 64.4°, 77.5° and 81.6° angle values for metallic silver peaks were observed. (ICSD Files PDF Card No: 01-087-0717). Peaks belonging to the crystal structures (111), (200), (311) and (220) corresponding to the angle values of 2θ=43.2°, 50.3°, 61.3° and 74.1° were observed for metallic copper. (ICSD Files PDF Card No: 01-070-3038). Moreover, it was concluded from the diffraction spectrum that the metals from the plant were found as impurities.

The results of TEM and SEM–EDX analyzes for the determination of the surface structures, sizes, crystal structures, shapes and elements of nanoparticles are given in Figs. 3 and 4, respectively. From the TEM images (Fig. 3), it is seen that the nanoparticles have a spherical crystal structure, monodisperse distribution and their average sizes are found to be 14.25±0.15, 10.23±0.22 and 5.81±0.08 nm for Ag NPs, Ag/Cu NPs and Cu NPs, respectively. In the TEM image of Ag/Cu NPs, dark parts indicate the presence of Cu, while lighter parts indicate the presence of Ag.

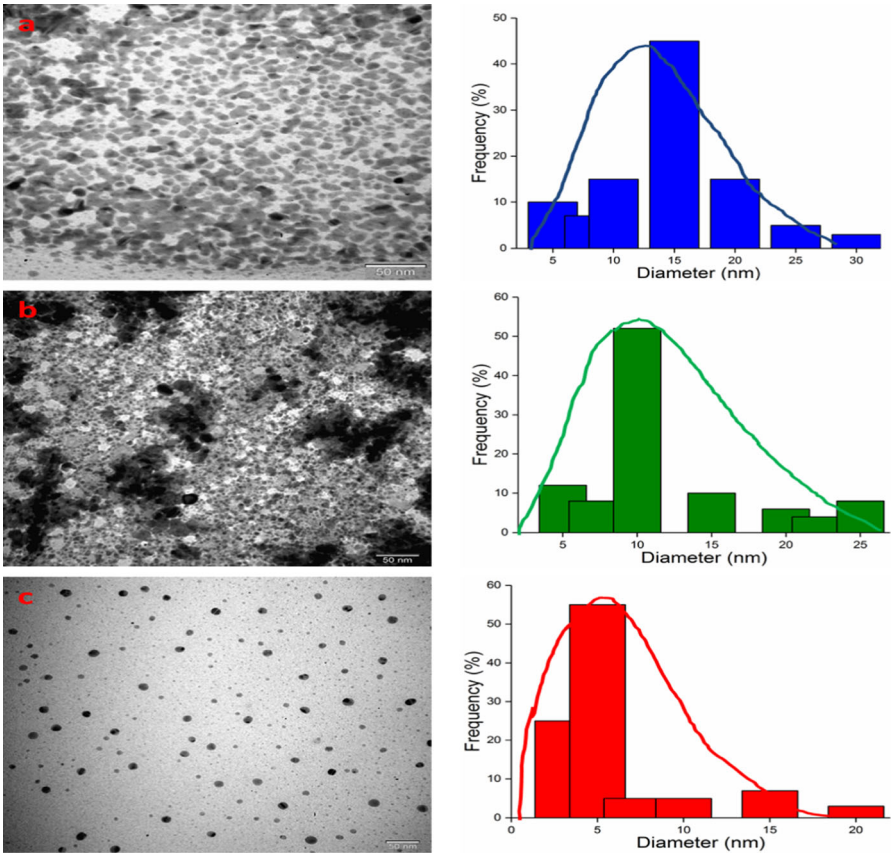

Fig. 3 From left to right TEM images and histograms of **a** Ag NPs, **b** Ag/Cu NPs and **c.** Cu NPs

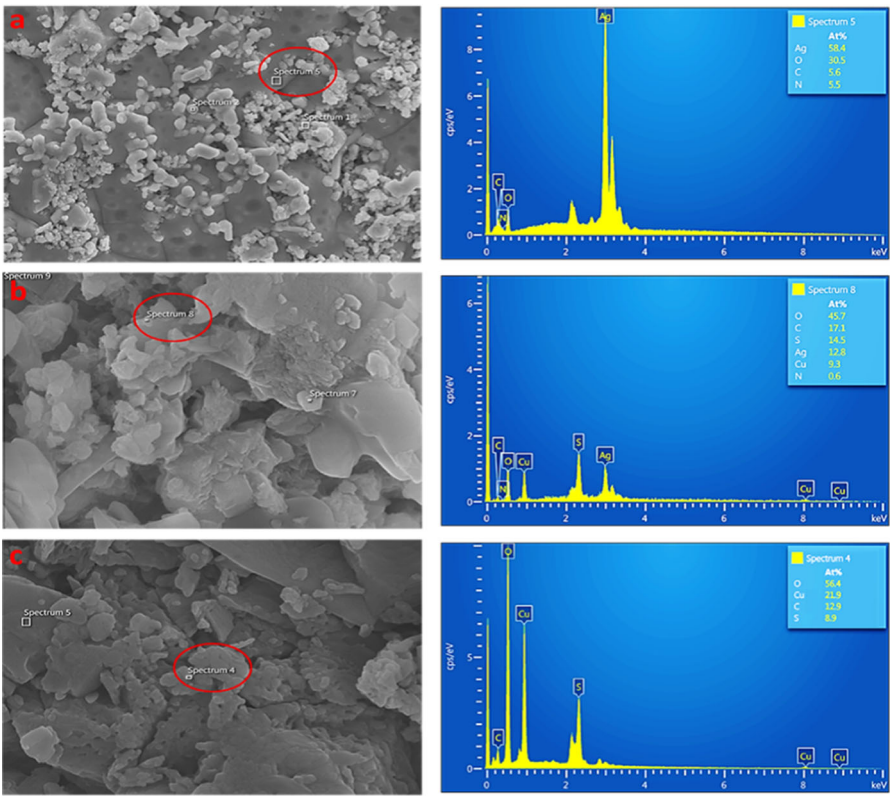

Fig. 4 SEM–EDX analysis of **a** Ag NPs, **b** Ag/Cu NPs and **c** Cu NPs

From this structure, it is seen that the Ag/Cu nanoparticle is stacked and layered in the heterojunction structure.

O, C and N seen in the EDX spectra (Fig. 4) of all nanoparticles originate from the plant extract and the FT-IR spectrum of the plant (Fig. 2a) also confirms this result. It is thought that the element S seen in the EDX spectra of Cu NPs and Ag/Cu NPs may originate from the $CuSO_4$ salt. From the SEM images (Fig. 4), the morphology of the nanoparticles is determined as irregular spherical and oval and it is seen that they are agglomerated.

The surface area, pore diameter and pore volume of the synthesized nanoparticles were calculated from the N_2 adsorption and desorption isotherm (Fig. 5) by the BJH (Barrett−Joyner−Halenda) method. As seen in Fig. 5, Cu NPs and Ag NPs follow the Type H3 hysteresis loop; possibly related to slit-shaped pores between parallel layers [36]. The obtained surface area (S_{BET}), micropore volume (V_{mic}), total pore volume (V_{Tot}) and pore diameters (D_p) data are given in Table 1. As seen in Table 1, although Ag NPs have the largest surface area, their pore diameters are low. On the other hand, Cu NPs have the highest micro and mesopore diameter. In general, IUPAC pores are classified into three categories according to their size as macropores ($d>50$ nm), mesopores ($2<d<50$ nm) and micropores ($d<2$ nm). As seen in Table 1 that based

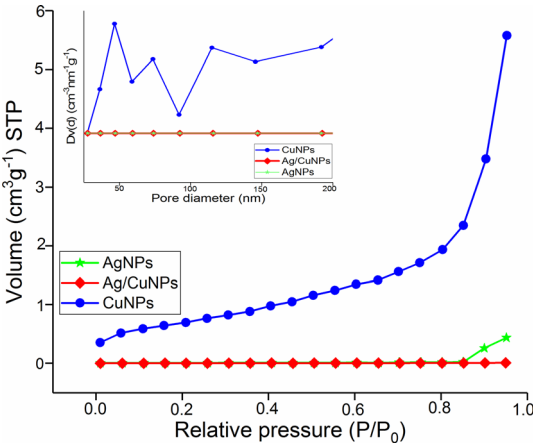

Fig. 5 BET isotherms and (inset) pore size distribution of Ag NPs, Ag/Cu NPs and Cu NPs

Table 1 Textural properties and particle size of the prepared catalysts/adsorbents

Properties	Ag NPs	Ag/Cu NPs	Cu NPs
Specific (BET) surface area (m^2 g^{-1})	8.2503	6.0127	6.8816
Total pore volume (BJH) (cm^3 g^{-1})	0.0062	0.0344	5.8311
Microporous pore volume (cm^3 g^{-1})	0.0012	0.0153	0.2381
Mesoporous pore volume (cm^3 g^{-1})	0.0048	0.0192	5.5930
Average pore size (BJH) (nm)	0.2500	0.2200	4.3700

on the pore size distribution calculated by the BJH method while the pore diameters of the Cu NPs are in the meso-range, that of both Ag NPs and Ag/Cu NPs are in the micropore range, and the average pore diameters are approximately equal to 4.37 nm, 0.25 nm and 0.22 nm, respectively.

Catalytic activity and adsorption performance of NPX, DCF and NPX+DCF onto nanocatalyst/nanoadsorbents

The adsorption and catalytic wet peroxidation in the presence of H_2O_2 as oxidation agent for 20 mg/L 50 mL of NPX, DCF and NPX+DCF were separately investigated and the results were given in Fig. 6a, b), respectively. During the experiment, 5 mL of the solutions after a certain period of time was taken and centrifuged and then absorbances in a solution were measured at 272 (λ_{NPX}) and 254 (λ_{DCF}) nm fixed wavelength in the UV–Vis spectrophotometer and the amounts of NPX and DCF were calculated from Eq. (1) using related the calibration plot for both adsorption and CWPO experiments and drug removal percentages were calculated using Eq. (2).

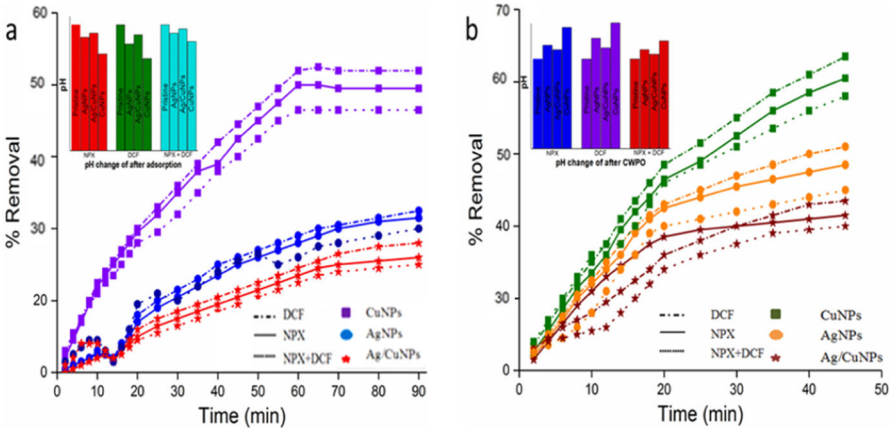

Fig. 6 **a** Adsorption of **b** CWPO of NPX, DCF and NPX+DCF onto Ag NPs, Ag/Cu NPs and Cu NPs (initial drug concentration: 20 mg/L, adsorbent dosage: 25 mg/50 mL, T=298 K, pH=4.5 (30% of 3 mL H_2O_2 for CWPO) and (inset) pH change of after adsorption and CWPO)

$$Q_e = \frac{(C_0 - C_e)V}{\mathrm{W}} \tag{1}$$

$$\mathrm{R}\ \% = \frac{(C_0 - C_e)}{C_0} * 100 \tag{2}$$

where C_0 and C_e are the initial and equilibrium concentrations (mg/L), respectively, V is the volume of drug solution (L), and W is the weight (g) of adsorbents.

As seen in Fig. 6, Cu NPs showed the best catalytic activity and adsorption performance in NPX, DCF and NPX+DCF removal. These results are in agreement with the BET analysis. In the removal of NPX, DCF and NPX+DCF with CWPO, 58%, 63% and 56% efficiencies were achieved by using Cu NPs nanocatalyst after 50 min, respectively. In the removal of NPX, DCF and NPX+DCF with adsorption, 49%, 54% and 45% efficiencies were achieved by using Cu NPs nanoadsorbent after 90 min, respectively. From the experimental data, it was observed that the adsorption was fast in the first minutes and slowed down over time. In order to get more effective efficiency in drug removal and to investigate the synergistic effect, the degradation studies were carried out by combining the CWPO process after 10 min of adsorption of the drugs; the data obtained are given in Fig. 7.

As can be seen in Fig. 7, in the removal of NPX, DCF and NPX+DCF by combining the CWPO process after 10 min' adsorption of the drugs, 84%, 91% and 75% efficiencies were achieved by using Cu NPs after 50 min, respectively. For the combining the CWPO with adsorption, Cu NPs were firstly added to the solutions including drugs and mixed with 10 min and then 3 mL of 30% H_2O_2 was added to the mixed solutions. These higher drug removal efficiencies with respect to adsorption and CWPO alone are thought to be due to the synergistic effect.

According to the pseudo-first-order kinetic model, t versus ln C values were plotted and the k_1 rate constant was determined from the slope. The plots obtained for

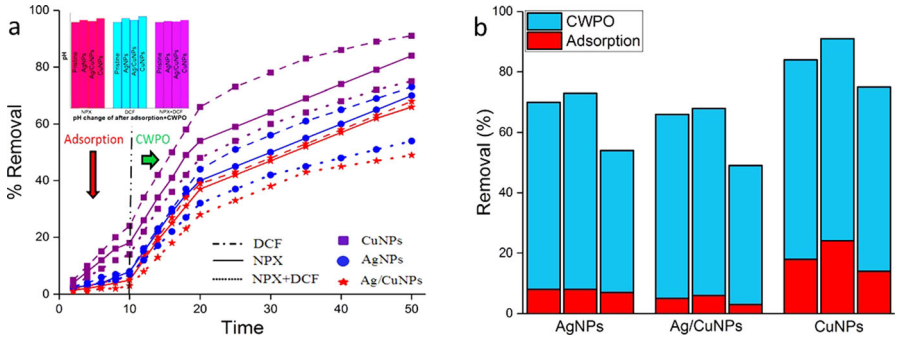

Fig. 7 **a** Degradation of NPX, DCF and NPX+DCF with adsorption+CWPO onto Ag NPs, Ag/Cu NPs and Cu NPs; (inset) pH change of after adsorption+CWPO and **b** adsorption and CWPO capacities of Ag NPs, Ag/Cu NPs and Cu NPs toward NPX, DCF and NPX+DCF

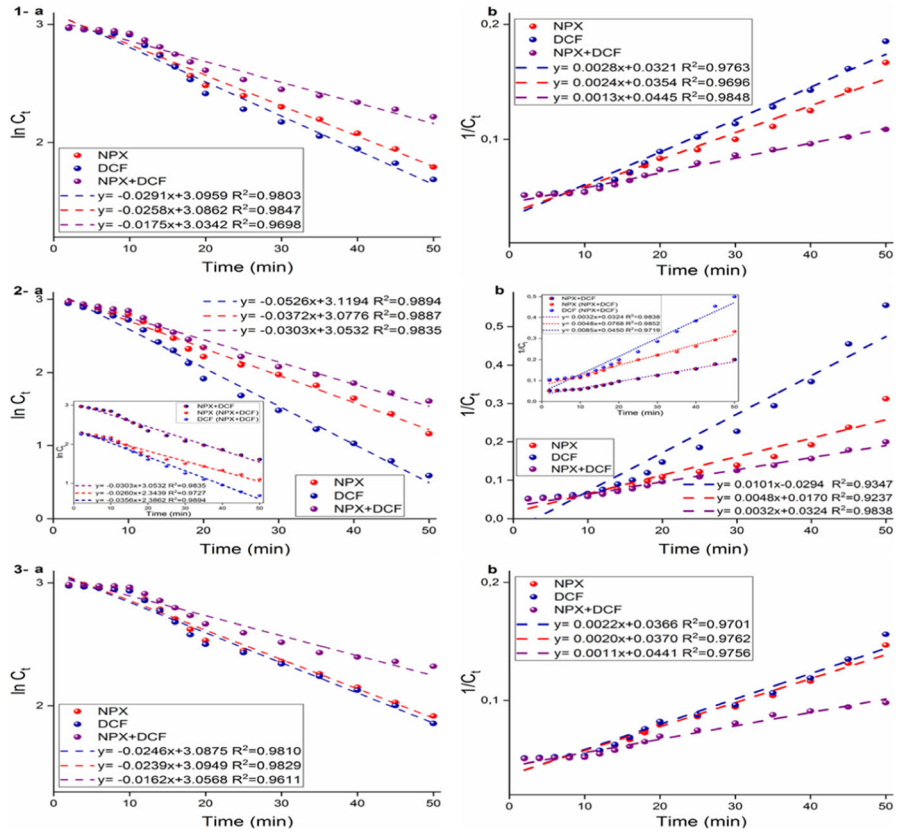

Fig. 8 Kinetics fittings plots for NPX, DCF and NPX+DCF adsorption+CWPO onto using **(1)** Ag NPs, **(2)** Cu NPs and **(3)** Ag/Cu NPs **a** pseudo-first-order, **b** pseudo-second-order kinetic models, respectively ($[NPX]_0$=20 mgL^{-1}, $[DCF]_0$=20 mgL^{-1} and $[NPX+DCF]_0$=20 mgL^{-1} (10 mgL^{-1} NPX+10 mgL^{-1} DCF), pH=4.5)

the pseudo-first-order kinetic model are given in Fig. 8a. According to the pseudo-second-order kinetic model, t versus $1/C$ values were plotted, and the k_2 rate constant was determined from the slope. The plots obtained for the pseudo-second-order kinetic model are given in Fig. 8b. The rate constants and coefficients of determination (R^2) calculated for the pseudo-first-order and pseudo-second-order kinetic models for all nanoparticles are shown in Fig. 8.

In Table 2, the kinetic data of the Cu NPs are given. When the coefficients of determination of the two kinetic models are compared, the values are close to each other but in the separate drug removal, the reaction kinetics is compatible with the pseudo-first-order kinetic model based on higher R^2 value. On the other hand, while in the both binary (NPX+DCF) and competitive NPX removal, the reaction kinetics is compatible with the pseudo-second-order kinetic model, in competitive DCF removal, the reaction kinetics is compatible with the pseudo-first-order kinetic model based on higher R^2 value.

In line with the results obtained from the binary competitive adsorption by CWPO and adsorption+CWPO experiments, in which NPX and DCF drugs were combined, it was revealed that all of the nanoparticles were more selective toward DCF (Fig. 7b). As a result, in competitive adsorption+CWPO experiments, the fact that the drug removal in the binary mixture is smaller than the sum of the individual adsorption of the components indicates that there is an antagonistic interaction between the components [37]. Figure 9a shows the structure of NPX and DCF and the removal rates in competitive adsorption+CWPO. The fact that the NPX molecule is more stable than the DCF molecule and the presence of –NH bond that can hydrogen bond in the DCF molecule suggest that it is effective in its selectivity. It is known that the hydrophobicity effect and the presence of nonpolar compounds increase the adsorption efficiency and tendency [38–40]. The DCF selectivity of the nanoadsorbent is a factor of the hydrophobicity (propensity to adsorption) octanol water separation coefficient (log Kow), which is an indicator, was found to be directly proportional (4.51>3.20). Furthermore the selectivity coefficient calculated from Eq. (3) is also ($S_{\mathrm{DCF/NPX}}$=6) confirms the result.

$$S_{A/B} = \frac{(C_{A1} - C_{A2})C_{B2}}{(C_{B1} - C_{B2})C_{A2}} \tag{3}$$

C_{A1} and C_{B1} are the initial drug concentrations. C_{A2} and C_{B2} are the remaining drug concentrations in the solution.

Table 2 Pseudo-first-order and pseudo-second-order model constants with the adsorption+CWPO technique of Cu NPs toward NPX, DCF and NPX+DCF

	Pseudo-first order		Pseudo-second order	
	k_1 (min^{-1})	R^2	k_2 (g L^{-1} min^{-1})	R^2
NPX	0.0372	0.9887	0.0048	0.9237
DCF	0.0526	0.9894	0.0101	0.9347
NPX+DCF	0.0303	0.9835	0.0032	0.9838
NPX(*competitive)*	0.0260	0.9727	0.0048	0.9852
DCF(*competitive)*	0.0356	0.9894	0.0085	0.9719

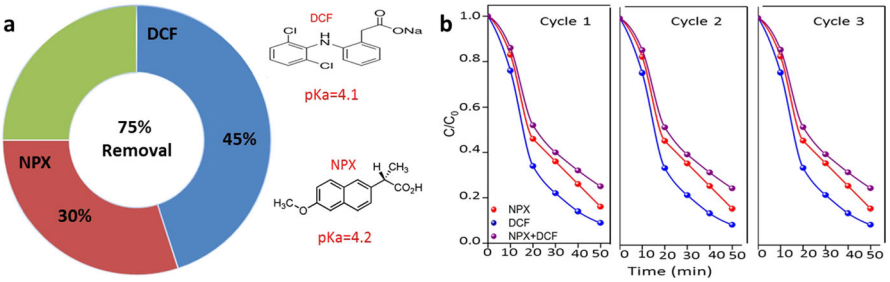

Fig. 9 **a** Competitive Ads+CWPO rates of Cu NPs and **b** recycling experiments for Ads+CWPO degradation of NPX, DCF and NPX+DCF using Cu NPs

In order to examine the reusability of the adsorbent/catalyst, the Cu NPs separated from the solution by filtration at the end of the experiment were reused for adsorption +CWPO processes and this process was repeated for 3 cycles. The results are given in Fig. 9b; It is seen that there is no significant decrease in the removal efficiencies in the 3rd cycle and the stable and active structure of the adsorbent/catalyst is preserved to the desired extent.

The oxidation and adsorption capacities of the nanocatalyst/nanoadsorbents synthesized in this study and the different catalyst/adsorbents in the literature for the degradation of pollutants are given in Table 3.

Adsorption/CWPO mechanism

Adsorption mechanisms generally involve the extensive effect of ion exchange, complexation, precipitation, electrostatic and π–π interaction types [50, 51]. In principle, it can be said that the decompositions of drugs by oxidation are based on the principle of producing $OH^{\cdot}$ radicals. H_2O_2 adsorbed by the metal nanoparticle takes electrons from the metal nanoparticle and forms $OH^{\cdot}$ radicals as a result of OH^{-} ion oxidation. These radicals adsorbed by the nanoparticle react with the drugs on the surface and cause the drugs to decompose. In other words, the $OH^{\cdot}$ radical oxidizes the drug and converts it to CO_2 and H_2O. The rate of catalytic oxidation depends on both adsorptions of H_2O_2 on the nanoparticle surface and electron transfer from the nanoparticle. It can be said that nanoparticles effectively weaken the O–O bond, providing an advantage for H_2O_2 adsorption and increasing the electron transport rate. In the literature, it has been explained that the possible oxidation reaction mechanism of pollutants occurs in the presence of hydroxyl ($HO^{\cdot}$) and hydroperoxyl ($HOO^{\cdot}$) radicals formed from H_2O_2 [34, 52]. Possible chemical interaction mechanism diagram according to functional groups is given in Fig. 10.

Conclusion

Metallic (Ag NPs, Cu NPs) and bimetallic nanoparticles (Ag/Cu NPs) were successfully synthesized for the first time using weed plant Helichrysum arenarium extract by an economical and environmentally friendly green synthesis method. The

Table 3 A comparison of the oxidation and adsorption capacities of the prepared catalyst/adsorbents with those announced in the literature

Pollutant	Adsorbent (A) or CWPO (C)	Adsorption capacity (mg/gr) or removal efficiency (%)	Time (min.)	References
Phenol	Fe-AC (C)	100%	240	[41]
Orange II	Fe_3O_4NPs (C)	70.5%	180	[42]
Bisphenol A	FeCu-MC (C)	93%	60	[43]
Naproxen	Fe/Ti-PB (C)	82%	120	[44]
Diclofenac	Fe_3O_4-MWCNT (C)	95%	180	[45]
Naproxen	Fe/Cu-AT (C)	84%	9	[33]
Diclofenac	Fe/Cu-CS (C)	92%	9	[33]
Methyl orange	Chitosan/organic rectorite-Fe_3O_4 (A)	5.56 mg/gr	80	[46]
Methyl orange	Fe_3O_4NPs (A)	132 mg/gr	60	[34]
Tetracycline	Fe/NiNPs (A)	93%	90	[47]
Tetracycline	PAC/Fe_3O_4 MNPs (C)	94.5%	180	[48]
Ibuprofen	Boron doped TiO_2 (UV+C)	95%	120	[49]
Naproxen	Cu NPs (A)	49%	90	Present study
Naproxen	Cu NPs (C)	58%	50	Present study
Naproxen	Cu NPs (A+C)	84%	50	Present study
Diclofenac	Cu NPs (A)	54%	90	Present study
Diclofenac	Cu NPs (C)	63%	50	Present study
Diclofenac	Cu NPs (A+C)	91%	50	Present study

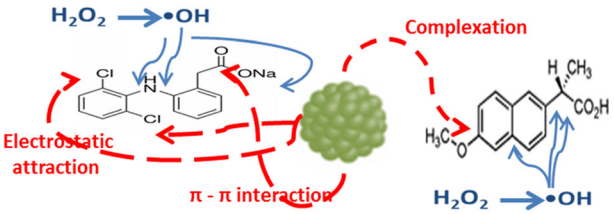

Fig. 10 Mechanisms scheme of NPX and DCF sorption/oxidation by Cu NPs

characterizations based on synthesis and structures of all nanoparticles were performed with TEM, SEM–EDX, XRD, FT-IR, UV–Vis and BET methods. It was observed that Cu NPs have the smallest particle size and the highest pore diameter. In this study, their use as innovative nanoadsorbent and nanocatalyst in the separately and/or together removal of nonsteroidal anti-inflammatory drugs, such as naproxen and diclofenac from the aqueous environment were investigated. Cu NPs provided the highest removal for both adsorption and CWPO processes. To realize drug removal with both faster and higher efficiency, the synergistic effect research studies were also carried out by combining the hybrid adsorption/CWPO processes in a way that CWPO process was applied after 10 min of adsorption. By doing this, it was observed that while drug removal was achieved in a higher efficiency with a shorter time compared to adsorption, it was observed that removal was achieved at the same time with higher efficiency than CWPO. In the removal of NPX, DCF and NPX+ DCF with CWPO, 58%, 63% and 56% efficiencies were achieved by using Cu NPs nanocatalyst after 50 min, respectively. In the removal of NPX, DCF and NPX+DCF with adsorption, 49%, 54% and 45% efficiencies were achieved by using Cu NPs nanoadsorbent after 90 min, respectively. In the removal of NPX, DCF and NPX+ DCF with hybrid adsorption/CWPO processes, 84%, 91% and 75% efficiencies were achieved by using Cu NPs after 50 min, respectively. Furthermore, in all experiments, it was observed that there was a selectivity against DCF and the efficiency was decreased compared to the single drug removal due to the interference effect in competitive drug removals. As a result of the kinetic studies, it was determined that the results were closer in competitive adsorption, where the reaction kinetics generally fit the pseudo-first-order kinetic model, and some of them fit the pseudo-second-order kinetic model. It was concluded that Cu NPs remained active in three times usage and could be used as an alternative adsorbent and catalyst in drug removal.

Author contributions Both authors contributed to the study conception and design. Material preparation, data collection and analysis were performed by Muradiye Şahin and Yasin Arslan. The first draft of the manuscript was written by Muradiye Şahin and both authors commented on previous versions of the manuscript. Both authors read and approved the final manuscript.

Funding This study was supported by Kırşehir Ahi Evran University Scientific Research Projects (FBE. A4. 22.001).

Data availability Not applicable.

Declarations

Conflict of interest The authors have no competing interests to declare that are relevant to the content of this article.

Ethical approval Not applicable.

References

1. M. Padervand, S. Ghasemi, S. Hajiahmadi, B. Rhimi, Z.G. Nejad, S. Karima, Z. Shahsavari, C. Wang, Appl. Catal. A-Gen. **643**, 118794 (2022)
2. M. Padervand, H. Heidarpour, M. Goshadehzehn, S. Hajiahmadi, Environ. Technol. Innov. **21**, 101212 (2021)
3. T. Azuma, N. Nakada, N. Yamashita, H. Tanaka, Chemosphere **93**, 1672 (2013)
4. R. Daghrir, P. Drogui, Environ. Chem. Let. **11**(3), 209 (2013)
5. N. Larsson, E. Petersson, M. Rylander, J.A. Jönsson, Anal. Methods. **1**(1), 59 (2009)
6. R.E. Green, I. Newton, S. Shultz, A.A. Cunningham, M. Gilbert, D.J. Pain, V. Prakash, J. Appl. Ecol. **41**(5), 793 (2004)
7. F. Orias, Y. Perrodin, Sci. Total Environ. **454**, 250 (2013)
8. M.A. Taggart, R. Cuthbert, D. Das, C. Sashikumar, D.J. Pain, R.E. Green, Y. Feltrer, S. Shultz, A.A. Cunningham, A.A. Meharg, Environ. Pollut. **147**(1), 60 (2007)
9. S. Silvestri, T.A. Burgo, C. Dias-Ferreira, J.A. Labrincha, D.M. Tobaldi, React. Funct. Polym. **146**, 104401 (2020)
10. V. Acuña, A. Ginebreda, J.R. Mor, M. Petrovic, S. Sabater, J. Sumpter, D. Barceló, Environ. Int. **85**, 327 (2015)
11. G.G. Song, Y.H. Seo, J.-H. Kim, S.J. Choi, J.D. Ji, Y.H. Lee, Z. Rheumatol. **75**, 508 (2016)
12. E. Koumaki, D. Mamais, C. Noutsopoulos, J. Hazard. Mater. **323**, 233 (2017)
13. V.M. Vulava, W.C. Cory, V.L. Murphey, C.Z. Ulmer, Sci. Total Environ. **565**, 1063 (2016)
14. N. Delgado, A. Capparelli, A. Navarro, D. Marino, J. Environ. Manage. **236**, 301 (2019)
15. N. Rafiei, A. Fatehizadeh, M.M. Amin, H.R. Pourzamani, A. Ebrahimi, E. Taheri, T.M. Aminabhavi, J. Environ. Manage. **297**(1), 113349 (2021)
16. K. Kasinathan, J. Kennedy, M. Elayaperumal, M. Henini, M. Malik, Sci. Rep. **6**, 38064 (2016)
17. H. Asakura, T. Matsuto, Waste Manage. **29**, 1852 (2009)
18. M. Yong, Y. Zhang, S. Sun, W. Liu, J. Membr. Sci. **575**, 50 (2019)
19. C. Noutsopoulos, E. Koumaki, D. Mamais, M. Nika, A. Bletsou, N. Thomaidis, Chemosphere **119**, 109 (2015)
20. S. Esplugas, D.M. Bila, L. Gustavo, T. Krause, M. Dezotti, J. Hazard. Mater. **149**(3), 631 (2007)
21. M. Padervand, S. Ghasemi, S. Hajiahmadi, C. Wang, Appl. Surf. Sci. **544**, 148939 (2021)
22. Y. Xin, Q. Zhu, T. Gao, X. Li, W. Zhang, H. Wang, D. Ji, Y. Huang, M. Padervand, F. Yu, C. Wang, Appl. Catal. B-Environ. **324**, 122238 (2023)
23. M. Padervand, B. Rhimi, C. Wang, J. Alloys Compd. **852**, 156955 (2021)
24. B. Czech, P. Oleszczuk, Chemosphere **149**, 272 (2016)
25. A. Karami, R. Sabouni, M. Ghommem, J. Mol. Liq. **305**, 112808 (2020)
26. Z.U.H. Khan, A. Khan, Y. Chen, N.S. Shah, N. Muhammad, A.U. Khan, K. Tahir, F.U. Khan, B. Murtaza, S. Hassan, S.A. Qaisrani, P. Wangi, J. Photochem. Photobiol. B Biol. **173**, 150 (2017)
27. A. Zaleska-Medynska, M. Marchelek, M. Diak, E. Grabowska, Adv. Colloid Interface Sci. **229**, 80 (2016)
28. X. Liu, D. Wang, Y. Li, Nano Today **7**, 448 (2012)
29. V.V. Makarov, A.J. Love, S.S. Makarova, I.V. Yaminsky, M.E. Taliansky, N.O. Kalinina, Acta Naturae. **6**(1), 35 (2014)
30. R. Komal, V. Arya, Int. J. Nanomater. Bios. **3**(1), 17 (2013)
31. A. Annamalai, S. Thomas Jose, N.A. Lyza, World Appl. Sci. J. **13**(8), 1833 (2011)
32. M. Şahin, Y. Arslan, F. Tomul, B. Yıldırım, H. Genç, React. Kinet Mech. Catal. **135**, 3303 (2022)
33. M. Şahin, Y. Arslan, F. Tomul, Res. Chem. Intermed. **48**, 5209 (2022)
34. M. Şahin, Y. Arslan, F. Tomul, Int. J. Environ. Anal. Chem. (2022). https://doi.org/10.1080/03067319.2022.2140417
35. M. Danish, X. Gu, S. Lu, A. Ahmad, M. Naqvi, U. Farooq, X. Zhang, X. Fu, Z. Miao, Y. Xue, Chem. Eng. Sci. **308**, 396 (2017)
36. G. Bharath, E. Alhseinat, N. Ponpandian, M.A. Khan, M.R. Siddiqui, F. Ahmed, E.H. Alsharaeh, Sep. Purif. Technol. **188**, 206 (2017)
37. V.C. Srivastava, I.D. Mall, I.M. Mishra, Chem. Eng. J. **117**, 79 (2006)
38. T. Atugoda, H. Wijesekara, D.R.I.B. Werellagama, K.B.S.N. Jinadasa, N.S. Bolan, M. Vithanage, Environ. Technol. Innov. **19**, 100971 (2020)

39. J. Rivera-Utrilla, G. Prados-Joya, M. Sánchez-Polo, M.A. Ferro-García, I. Bautista-Toledo, J. Hazard. Mater. **170**(1), 298 (2009)
40. A.M. Aljeboree, A.N. Alshirifi, J. Pharm. Sci. Res. **10**(9), 2252 (2018)
41. J.A. Zazo, J.A. Casas, A.F. Mohedano, J.J. Rodríguez, Appl. Catal. B **65**, 261 (2006)
42. N.A. Zubir, C. Yacou, J. Motuzas, X. Zhang, J.C. Dosta, Sci. Rep. **4**, 4594 (2014)
43. Y. Wang, H. Zhao, G. Zhao, Appl. Catal. B **164**, 396 (2015)
44. F. Tomul, Y. Arslan, E. Kendüzler, Int. J. Adv. Sci. Eng. Technol. **5**, 48 (2017)
45. Y. Huaccallo, S. Alvarez-Torrellas, M.P. Marin, M.V. Gil, M. Larriba, V.I. Agueda, G. Ovejero, J. Garcia, Environ. Sci. Pollut. Res. **26**, 22372 (2019)
46. L. Zeng, M. Xie, Q. Zhang, Y. Kang, X. Guo, H. Xiao, Y. Peng, J. Luo, Carbohydr. Polym. **123**, 89 (2015)
47. K.V.G. Ravikumar, S.V. Sudakaran, K. Ravichandran, M. Pulimi, C. Natarajan, A. Mukherjee, J. Clean. Prod. **210**, 767 (2019)
48. N. Jaafarzadeh, B. Kakavandi, A. Takdastan, R.R. Kalantary, M. Azizi, S. Jorfi, RSC Adv. **5**, 84718 (2015)
49. E.B. Simsek, Appl. Catal. B-Environ. **200**, 309 (2017)
50. G.X. Yang, H. Jiang, Water Res. **48**, 396 (2014)
51. H. Jin, M.U. Hanif, S. Capareda, Z. Chang, H. Huang, Y. Ai, J. Environ. Chem. Eng. **4**(1), 365 (2016)
52. J. Han, H.Y. Zeng, S. Xu, C.R. Chen, X.J. Liu, Appl. Catal. A Gen. **527**, 72 (2016)

Authors and Affiliations

Muradiye Şahin[1] Yasin Arslan[2]

Yasin Arslan
yasinarslan@mehmetakif.edu.tr

[1] Kırşehir Ahi Evran University, 40100 Kırşehir, Turkey

[2] Department of Nanoscience and Nanotechnology, Faculty of Arts and Science, Burdur Mehmet Akif Ersoy University, 15030 Burdur, Turkey